

Relative contributions of anomalous heat fluxes and effective heat capacity to sea surface temperature variability

Naoya Takahashi¹, Kelvin J Richards¹, Niklas Schneider¹, Malte Fabian Stuecker¹, H Annamalai², and Masami Nonaka³

¹University of Hawaii at Manoa

²IPRC

³Japan Agency for Marine-Earth Science and Technology

February 27, 2023

Abstract

Sea surface temperatures (SSTs) vary not only due to heat exchange across the air-sea interface but also due to changes in effective heat capacity as primarily determined by mixed layer depth (MLD). Here, we investigate seasonal and regional characteristics of the contribution of MLD anomalies to SST variability using observational datasets. We propose a metric called Flux Divergence Angle (FDA), which can quantify the relative contributions of surface heat fluxes and MLD anomalies to SST variability. Using this metric, we find that MLD anomalies tend to amplify SST anomalies in the extra-tropics, especially in the eastern ocean basins, during spring and summer. This amplification is explained by a positive feedback loop between SST and MLD via upper ocean stratification. In contrast, MLD anomalies tend to suppress SST anomalies in the eastern tropical Pacific. The MLD contribution in the summer hemispheres is more pronounced on seasonal timescales than on sub-monthly timescales.

Hosted file

955603_0_art_file_10705952_rq1h1t.docx available at <https://authorea.com/users/533589/articles/625151-relative-contributions-of-anomalous-heat-fluxes-and-effective-heat-capacity-to-sea-surface-temperature-variability>

Hosted file

955603_0_supp_10679598_rp19xp.docx available at <https://authorea.com/users/533589/articles/625151-relative-contributions-of-anomalous-heat-fluxes-and-effective-heat-capacity-to-sea-surface-temperature-variability>

1
2 **Relative contributions of anomalous heat fluxes and effective heat capacity**
3 **to sea surface temperature variability**
4

5 **Naoya Takahashi¹, Kelvin J. Richards^{1,2}, Niklas Schneider^{1,2}, Malte F. Stuecker^{1,2},**
6 **H. Annamalai^{1,2}, and Masami Nonaka³**

7 ¹ International Pacific Research Center, School of Ocean and Earth Science and Technology,
8 University of Hawai‘i at Mānoa, Honolulu, HI, USA

9 ² Department of Oceanography, School of Ocean and Earth Science and Technology, University
10 of Hawai‘i at Mānoa, Honolulu, HI, USA

11 ³ Japan Agency for Marine-Earth Science and Technology, Yokohama, Kanagawa, Japan
12
13

14 Corresponding author: Naoya Takahashi (naoyat@hawaii.edu)
15

16 **Key Points:**

- 17 ● Relative contributions of mixed layer depth (MLD) anomaly to SST variability are
18 investigated using the Flux Divergence Angle (FDA) metric.
- 19 ● MLD anomalies tend to amplify SST anomalies in the extra-tropics, especially in eastern
20 ocean basin, during the spring and summer seasons.
- 21 ● The contribution of MLD anomalies in the extra-tropics during summer is more
22 pronounced on seasonal timescales than on sub-monthly ones.
23

24 **Abstract**

25 Sea surface temperatures (SSTs) vary not only due to heat exchange across the air-sea interface
26 but also due to changes in effective heat capacity as primarily determined by mixed layer depth
27 (MLD). Here, we investigate seasonal and regional characteristics of the contribution of MLD
28 anomalies to SST variability using observational datasets. We propose a metric called Flux
29 Divergence Angle (FDA), which can quantify the relative contributions of surface heat fluxes
30 and MLD anomalies to SST variability. Using this metric, we find that MLD anomalies tend to
31 amplify SST anomalies in the extra-tropics, especially in the eastern ocean basins, during spring
32 and summer. This amplification is explained by a positive feedback loop between SST and MLD
33 via upper ocean stratification. In contrast, MLD anomalies tend to suppress SST anomalies in the
34 eastern tropical Pacific. The MLD contribution in the summer hemispheres is more pronounced
35 on seasonal timescales than on sub-monthly timescales.

36

37 **Plain Language Summary**

38 Sea surface temperatures (SST) is one of the important indicators as well as drivers of climate
39 variability over the globe. SST varies not only due to changes in surface heat fluxes but also due
40 to changes in effective heat capacity as mainly determined by mixed layer depth (MLD)
41 anomalies. In this study, we propose a new metric called “Flux Divergence Angle (FDA)”,
42 which can quantify the relative contributions of MLD and surface heat flux anomalies to the
43 SST variability. Using this metric, we find that the MLD anomaly tends to amplify the local SST
44 variability in the extra-tropics (especially in the eastern ocean basins) and during spring and
45 summer. On the other hand, MLD anomalies tend to suppress the SST variability in the eastern
46 tropical Pacific. Changes in effective heat capacity in the summer hemispheres are more
47 important for slower SST variability (e.g., for several months) than that for faster one (e.g., for
48 several days).

49

50 **1 Introduction**

51 Sea surface temperature (SST) is one of the key metrics as well as drivers of climate
52 variability over the globe. Surface heat flux (SHF) is known as the most fundamental factor
53 causing local SST variations in most of the extra-tropics (Hasselmann 1976; Frankignoul and
54 Hasselmann 1977). Mixed layer depth (MLD) is in turn another key factor determining the
55 effective heat capacity of the ocean surface layer, which also affects local SST variations (e.g.,
56 Alexander et al., 2000; Alexander & Penland, 1996; Amaya et al., 2021; Morioka et al., 2011;
57 Qiu & Kelly, 1993; Takahashi et al., 2021; Yamamoto et al., 2020; Yokoi et al., 2012). More
58 specifically, positive SST anomalies can be caused without SHF anomaly, if there is shallow
59 MLD anomaly with climatological heating (and vice versa). Therefore, not only the flux of heat
60 across the air-sea interface is important, but also how this heat is re-distributed within the mixed
61 layer.

62 Based on a mixed layer temperature budget from in-situ observations, previous studies
63 have shown that shallow MLD anomalies can cause positive SST anomalies especially in spring
64 and summer when MLD is shallow and climatological surface heating exists (Alexander et al.,
65 2000; Alexander & Penland, 1996; Cronin et al., 2013; Elsberry & Garwood, 1978; Lanzante &

66 Harnack, 1983). A part of the role of MLD anomalies has been revealed, however, a global
67 picture of the relative importance of MLD anomalies in SST variability is missing. In the
68 present, we can assess details of the role of MLD using various global datasets of vertical
69 oceanic properties, such as Argo float observations. For example, Tozuka et al. (2018) proposed
70 a metric for the relative importance of SHF and MLD anomalies to frontogenesis and frontolysis
71 respectively based on Argo float data, finding that seasonal variations of the horizontal gradient
72 of MLD strongly contribute to the strength of the SST front. In the present study, we revisit the
73 relative importance of MLD and SHF anomalies to SST variability and explore their seasonal
74 and regional characteristics over the global oceans.

75 The key scientific questions are “How large is the contribution of MLD anomalies to SST
76 variability compared to the contribution of SHF anomalies?” and “When/Where are they most
77 important?”. To answer these questions, we 1) propose a metric for quantifying the relative
78 contributions of SHF and MLD anomalies to the month-to-month variations of local SST
79 anomalies and 2) reveal their seasonal (e.g., summer *vs.* winter) and regional characteristics (e.g.,
80 tropics *vs.* extra-tropics). Furthermore, potential timescale dependences of their contributions are
81 explored using high-temporal oceanic reanalysis datasets.

82 The remainder of the paper is organized as follows. In section 2, we describe the datasets
83 used in this study, and propose a metric to quantify the relative contributions of SHF and MLD
84 anomalies to local SST variability. In section 3, we present the results on seasonality, regionality,
85 and timescale dependence of the relative contribution of MLD anomaly. In section 4, we
86 summarize our results and discuss the role of MLD anomalies in major climate modes.

87

88 2 Datasets and Methods

89 2.1 Datasets

90 In this study, we utilize three variables; SST, SHF, and MLD. Each variable is obtained
 91 from observational data sources; CERES-EBAF (Loeb et al., 2018) for radiative fluxes, OAFflux
 92 (Yu et al., 2008) for turbulent heat fluxes, OISST (Reynolds et al., 2002) for SST, and IPRC-
 93 Argo products (<http://apdrc.soest.hawaii.edu/projects/argo/>) for MLD. MLD is defined as the
 94 depth at which density increases from 10-m to the value equivalent to a temperature decrease of
 95 0.2 °C. All variables are monthly-averaged, for 15 years from January 2005 to December 2019.
 96 The horizontal resolution of all variables is 1 degree in both zonal and meridional directions. In
 97 the latter part of the section 3, we examine the timescale dependence of the relative contributions
 98 of MLD and SHF using 5-day mean variables from the SODA 3.4.2 ocean reanalysis dataset
 99 (Carton et al., 2018), which is forced by the ERA-Interim dataset (Dee et al., 2011). While the
 100 seasonality and regionality of the relative contributions in the SODA dataset are slightly different
 101 from those in the observational datasets (cf. Figs. 2 vs. S2 and Figs. 3 vs. S3), our main
 102 conclusions are not sensitive to these different data sources.

103

104 2.2 Metric to determine the relative contributions of SHF and MLD anomalies to local SST 105 variability

106 Here, we propose a metric to quantify the relative contributions of SHF and MLD
 107 anomalies to local SST variability. We start to develop the metric from the simplified mixed
 108 layer temperature budget equation (Qiu & Kelly, 1993) considering only surface forcing:

$$\frac{\partial T}{\partial t} = \frac{Q}{\rho c_p H} + \varepsilon_o, \quad (1)$$

109 where ρ is the density of sea water, c_p the specific heat capacity at constant pressure, H is MLD,
 110 and ε_o is the sum of contributions from all other oceanic processes (i.e., three-dimensional
 111 advection, entrainment, and diffusion) and the residual derived from unresolved processes and
 112 observational error. T is vertical mean temperature within the mixed layer. In this study, we
 113 assume that T is equivalent to SST. Q is the surface heat flux into the mixed layer (i.e., SHF) and
 114 calculated as the difference between net surface heat flux (Q_0) and penetrative SW radiation at
 115 the bottom of mixed layer (q_{pen}); $Q = Q_0 - q_{pen}$. The q_{pen} is calculated following Paulson &
 116 Simpson (1977). Hereafter, we focus on month-to-month SST variations and define anomalies of
 117 all variables as the deviations from the climatology at each grid point. Considering the heat
 118 budget equation for T anomalies, we can decompose the anomalies of the first term on the right-
 119 hand-side (rhs) of equation (1) into contributions from SHF and MLD anomalies (Morioka et al.,
 120 2010; Yokoi et al., 2012). We can rewrite the heat budget equation:

$$\frac{\partial T'}{\partial t} \sim \frac{Q'}{\rho c_p \bar{H}} - \frac{\bar{Q} H'}{\rho c_p \bar{H}^2} + \varepsilon_o', \quad (2)$$

121 where overbars (\bar{X}) and primes (X') denote the seasonal climatology and anomalies, respectively.
 122 The first term on the rhs represents the contribution of the SHF anomaly (Q') acting on a
 123 constant MLD (\bar{H}) and the second term represents the contribution of the MLD anomaly (H')
 124 under climatological heating/cooling (\bar{Q}). We ignore second and higher order terms of the Taylor

125 Expansion in equation (2) (e.g., the non-linear contribution of both anomalies) because they are
 126 typically much smaller than the sum of the first two terms ($\sim 1/10$), except in the Antarctic
 127 Circumpolar Current (ACC) region and the Labrador sea where the subduction zone of the
 128 Atlantic Meridional Overturning Circulation is located. The first two terms can explain more
 129 than 90 % of the total variances of the surface forcing term in most of the region (Fig. S1).

130 Next, we formulate a temperature variance budget equation (Boucharel et al., 2015; Guan
 131 et al., 2019; Santoso et al., 2010) by multiplying the SST anomaly (T') on both sides of equation
 132 (2):

$$T' \frac{\partial T'}{\partial t} = T' \left(\frac{Q'}{\rho c_p \bar{H}} - \frac{\bar{Q} H'}{\rho c_p \bar{H}^2} + \varepsilon_o' \right), \quad (3)$$

$$T' \frac{\partial T'}{\partial t} = \frac{1}{\rho c_p \bar{H}} \left(Q' T' - H' \frac{\bar{Q}}{\bar{H}} T' \right) + \varepsilon_o' T'. \quad (4)$$

133 The left-hand-side of the equations are equivalent to half of the time tendency of T' squared,
 134 hence we can diagnose the dominant processes that result in an increase or decrease of the T'
 135 variance. The reason why we employ the heat variance budget equation (Eq. 4) instead of the
 136 heat budget equation (Eq. 2) is that the role of surface forcing processes in the SST evolution can
 137 be captured by the variance budget equation.

138 As noted in section 1, Tozuka et al. (2018) proposed a metric for quantifying the relative
 139 contribution of horizontal gradients of SHF and MLD to the seasonal variation of frontogenesis.
 140 The method is analogous to the so-called ‘‘Turner angle’’ (Ruddick, 1983; You, 2002) which can
 141 be used to diagnose relative contributions of vertical gradients of temperature and salinity to
 142 double-diffusive convection. Here, following the basic concepts of these two studies, we define a
 143 new metric called Flux Divergence Angle (FDA; Θ), which quantifies the relative contributions
 144 of SHF and MLD anomalies to local SST variability:

$$\Theta = \tan^{-1}(Q_Q - Q_H, Q_Q + Q_H), \quad (5)$$

145 where

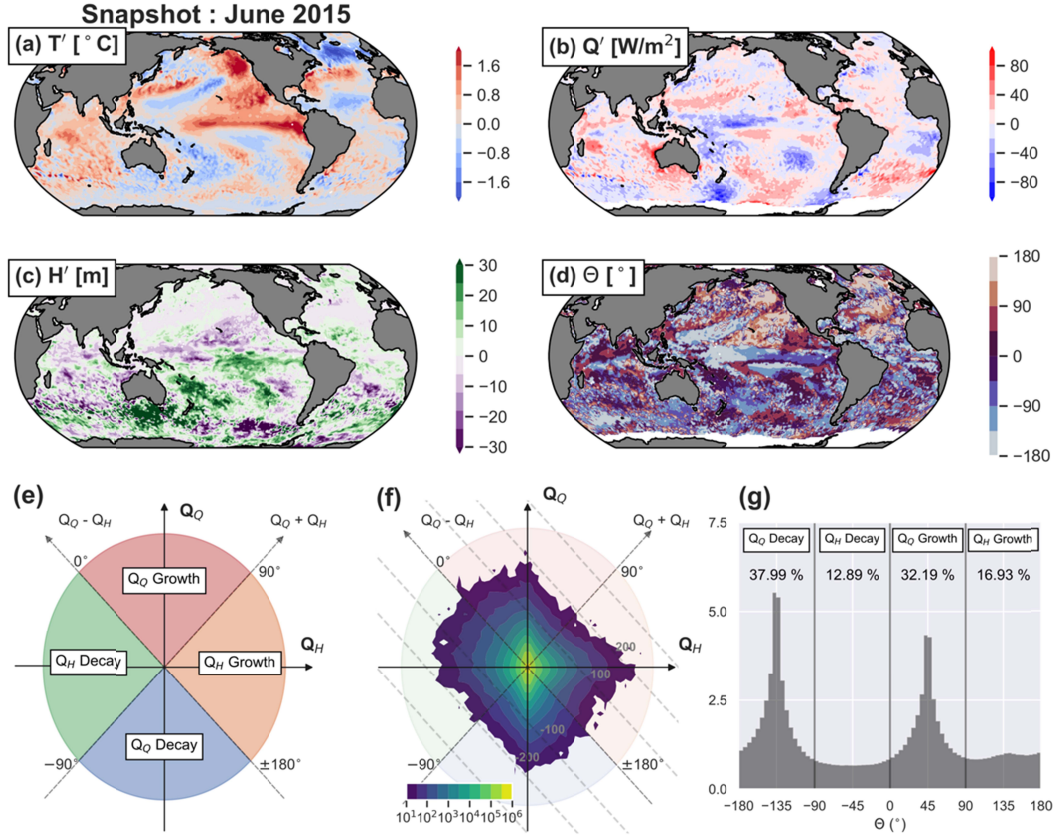
$$Q_Q = Q' T', \quad Q_H = -H' \frac{\bar{Q}}{\bar{H}} T'.$$

146 The two indices of Q_Q and Q_H are a part of the equation (4), have the same unit of $K \cdot W/m^2$, and
 147 represent the product of anomalies of SST and SHF (or the product of anomalies of SST and
 148 equivalent heat flux anomalies due to a MLD anomaly with climatological heating/cooling) .
 149 Positive and negative values of these indices represent that the heat flux anomalies amplify and
 150 dampen the local SST anomalies, respectively. Figures 1a to 1c are snapshots of SST, SHF, and
 151 MLD anomalies on June 2015. In addition, a snapshot of FDA on June 2015 is shown in Fig. 1d,
 152 calculated via equation (5) at each grid point. Figure 1f shows a two-dimensional histogram of
 153 all pairs of Q_Q and Q_H , showing that there is no apparent linear relationship between them.

154 Next, we illustrate the physical meaning of the FDA using a schematic in Figure 1e.
 155 When the FDA has a positive value, i.e., when the sum of Q_Q and Q_H is positive, the covariance
 156 of total surface forcing and SST anomaly is positive, so that the surface forcing term in equation
 157 (4) acts to amplify the local SST anomalies. This is referred to as ‘‘Growth’’ stage of the SST

158 evolution by surface forcing. Analogous, when the FDA has a negative value, i.e., when the sum
159 of Q_Q and Q_H is negative, the covariance of total surface forcing and SST anomaly is negative, so
160 that the surface forcing term in equation (4) acts to dampen the local SST anomalies (“Decay”
161 stage). Additionally, when the relative contribution of SHF is larger than that of MLD, FDA has
162 a specific value range of $0^\circ < \theta < 90^\circ$ for the “Growth” stage and $-180^\circ < \theta < -90^\circ$ for
163 the “Decay” stage. In contrast, when the contribution of MLD is larger than that of SHF, FDA
164 has the range of $90^\circ < \theta < 180^\circ$ for the “Growth” and $-90^\circ < \theta < 0^\circ$ for the “Decay” stage.
165 Depending on the relative importance, we add the header of “ Q_Q ” or “ Q_H ” before the name of
166 “Growth” or “Decay” stage, e.g., “ Q_Q Growth” when $0^\circ < \theta < 90^\circ$. Note that a term of
167 “dominant” in the following text indicates their relative importance of the SHF and MLD terms
168 but not necessarily their absolute importance relative to other terms in the full variance heat
169 budget. For example, upwelling and lateral advection have large impacts on SST variability in
170 the eastern tropical Pacific and in western boundary current regions, respectively. In such cases,
171 surface forcing processes are less important than oceanic processes. Hence, the term “dominant”
172 used in this manuscript refers to only the relative importance of the SHF anomaly or MLD
173 anomaly among the surface forcing processes.

174



175

176 **Figure 1 : Snapshots of horizontal maps of (a) SST anomaly, (b) SHF anomaly, (c) MLD anomaly, and (d)**
 177 **FDA on June 2015. (e) Schematic diagram of the four sectors (“Q_Q Decay”/ “Q_H Decay” / “Q_Q Growth” / “Q_H**
 178 **Growth”) diagnosed by the FDA metric. (f) Two-dimensional histogram of Q_Q and Q_H using all pairs over the**
 179 **global ocean and in all seasons. Units of Q_Q and Q_H are K*W/m². Bin size is 10 K*W/m² for both Q_Q and Q_H.**
 180 **Only count numbers greater than 10 are displayed. Dashed contours where Q_Q+ Q_H =-300, -200, -100, 0, 100,**
 181 **200, 300 are also plotted. (g) Histogram of FDA normalized by total count numbers (Unit: %) using a bin size**
 182 **of 5°. Numbers below each label indicate the occurrence frequency in each sector (Unit: %).**

183

184 To further investigate the regional characteristics of the FDA histogram (Fig. 1g), we
 185 calculate the occurrence frequencies of the four sectors (F_i) at each grid point during specific
 186 seasons as below,

$$F_i(x, y) = \frac{N_i(x, y)}{N_{ALL}}, \quad \begin{cases} i = 1 : -180^\circ \leq \theta < -90^\circ \\ i = 2 : -90^\circ \leq \theta < 0^\circ \\ i = 3 : 0^\circ \leq \theta < 90^\circ \\ i = 4 : 90^\circ \leq \theta < 180^\circ \end{cases} \quad (6)$$

187 where N_i is the count number of events with a specific value range of FDA. N_{ALL} is the total
 188 count number at each grid point, which is 45 for each season (i.e., each 3-month seasonal
 189 average during 15 years). Horizontal maps of F_i tell us the regionality of the dominant processes
 190 for the local SST evolution at each grid point.

191

192 3 Results

193 3.1 Global characteristics of FDA

194 First, we provide an overview of the general characteristics of the FDA using all pairs of
 195 Q_Q and Q_H over the global ocean and in all seasons. Figure 1g shows a histogram of FDAs
 196 normalized by total count numbers. The number below each label in Figure 1g indicates the
 197 occurrence frequency of each sector. The histogram has two sharp peaks at around 45° and -135° .
 198 The occurrence frequency of “ Q_Q Growth” is 32.19 % and that of “ Q_Q Decay” is 37.99 %. These
 199 results demonstrate that SHF anomalies are the main factor determining anomalies of the total
 200 surface forcing term. This is consistent with previous results on the relationship between SHF
 201 and SST, i.e., SST anomalies can be caused by wind or radiative forcing and can be dampened
 202 by heat release from the sea surface (Hasselmann, 1976). Although the SHF anomalies are the
 203 main driver of the SST anomalies in most of the cases investigated here, in some cases MLD
 204 anomalies contribute more to the SST anomalies than the SHF anomalies. For example, FDA
 205 around Hawaii on June 2015 (Figure 1d) had positive values greater than 90° (i.e., light reddish
 206 color shading), suggesting that the SST anomalies were primarily determined by the “ Q_H
 207 Growth” process rather than “ Q_Q Growth” and “ Q_Q Decay”. In the next subsection, we further
 208 explore the regional and seasonal characteristics of the “ Q_H Growth” and “ Q_H Decay” processes.

209

210 3.2 Regional and seasonal characteristics of FDA

211 Figure 2 shows the FDA histograms for each ocean basin (Pacific, Atlantic, and Indian
 212 Ocean), different regions (Northern Hemisphere [NH], Equatorial region [EQ], and Southern
 213 Hemisphere [SH]), and different seasons (December-January-February [DJF], March-April-May
 214 [MAM], June-July-August [JJA], and September-October-November [SON]). Maps of the
 215 occurrence frequency of the four sectors in each season are also shown in Figure 3. Hereafter, we
 216 will describe the details of the relative contributions of MLD anomalies (“ Q_H Growth” and “ Q_H
 217 Decay”) compared to the contribution of SHF anomalies (“ Q_Q Growth” and “ Q_Q Decay”). The
 218 contribution of SHF anomalies is dominant all over the global ocean (Fig. 2a-h), especially in
 219 most of the extra-tropical regions and in winter (Fig. 3a,c,e,g,i,k,m,o).

220

221 3.2.1 Q_H Growth process

222 In the extra-tropics (Fig. 2a,b,f,g,h), the histograms show a clear seasonal difference
 223 between summer and winter. In the winter hemisphere (i.e., JJA in the NH and DJF in the SH),
 224 occurrence frequencies of “ Q_Q Growth” and “ Q_Q Decay” are larger than those of “ Q_H Growth”
 225 and “ Q_H Decay”. While occurrence frequencies of “ Q_Q Growth” and “ Q_Q Decay” are also large
 226 in summer, however, occurrence frequency of “ Q_H Growth” in spring and summer is clearly
 227 larger than in winter. This suggests that the contribution of MLD anomalies is more pronounced
 228 in the spring and summer seasons than in the winter season, which is consistent with previous
 229 research (Alexander et al., 2000; Alexander & Penland, 1996; Cronin et al., 2013; Elsberry &
 230 Garwood, 1978; Lanzante & Harnack, 1983). The “ Q_H Growth” sector reflects the negative
 231 covariance between anomalies of SST and MLD under climatological heating. In this situation,
 232 MLD decreases with enhanced upper ocean stratification due to the increase in SST and/or

233 decrease in sea surface salinity (i.e., decrease in the surface water density). On the other hand,
234 SST easily increases under a shallow MLD anomaly and climatological surface heating in the
235 summer hemisphere. Thus, during summer, this positive feedback loop between MLD and SST
236 anomalies can amplify the local SST anomalies.

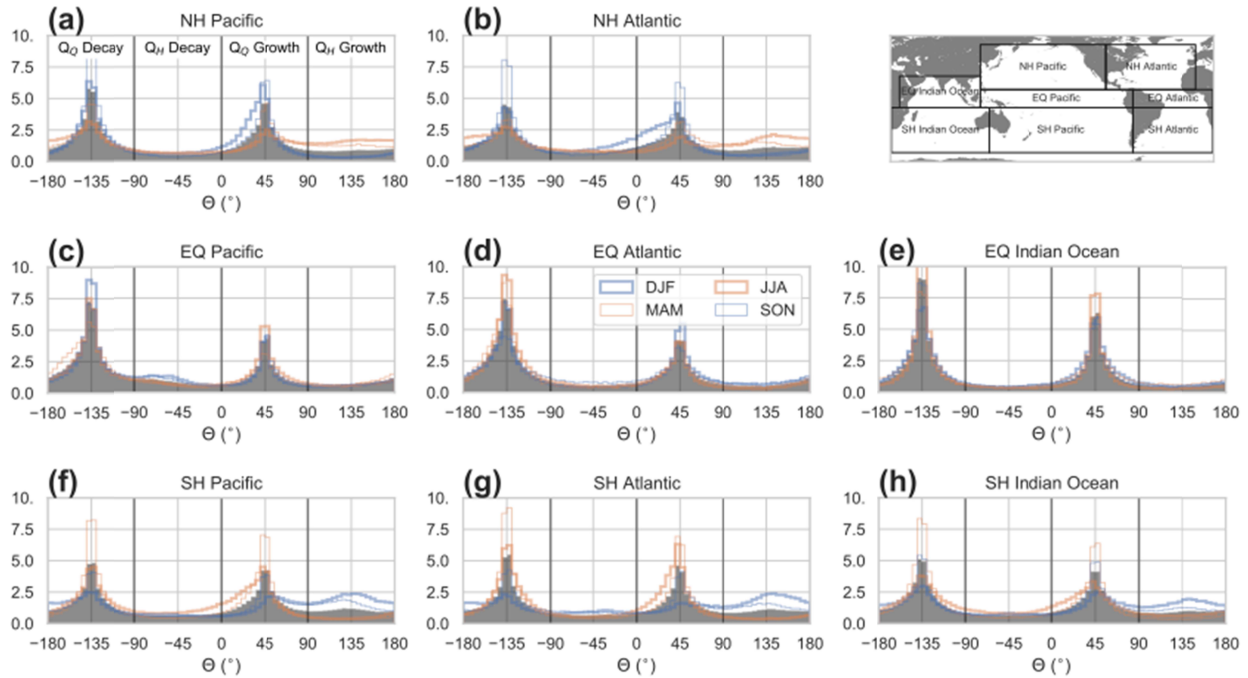
237 As noted in the previous paragraph, the “ Q_H Growth” sector is dominant in the summer
238 hemisphere, particularly in the eastern part of the ocean basins (Fig. 3d,h,l,p). The region with a
239 large contribution of MLD anomalies exhibits a horseshoe-like pattern, especially in the North
240 Pacific (Fig. 3h,l). One reason for the large contribution of MLD anomalies is large variability of
241 MLD anomalies in subtropical regions (Fig. S4a), particularly due to strong surface friction
242 velocity in the subtropical Pacific (Zhu & Zhang, 2018). Another reason is a large value of the
243 ratio of mean SHF to mean MLD in the North Pacific and Atlantic ($> 50^\circ\text{N}$ in Fig. S4b), which
244 is mainly due to the shallow climatological mean MLD under the strong climatological heating at
245 the sea surface (Fig. S4c, d).

246

247 3.2.2 Q_H Decay process

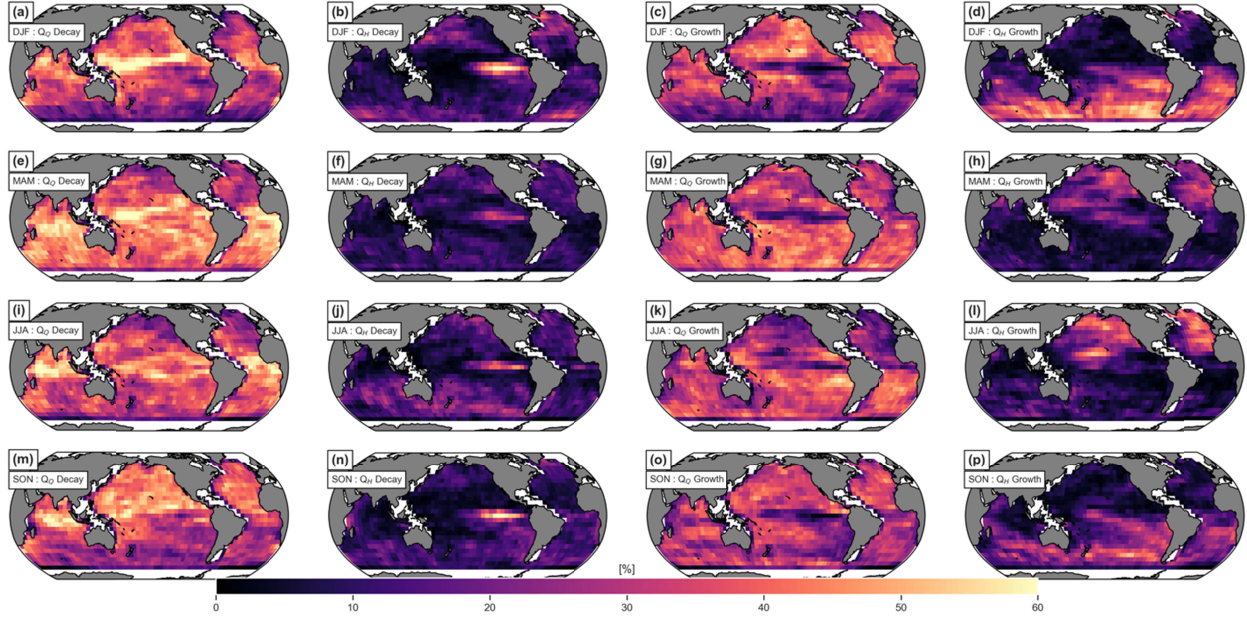
248 While the contribution of SHF anomalies is dominant in most of the tropics (Fig. 2c,d,e),
249 there is a small peak of occurrence frequency of “ Q_H Decay” in the EQ Pacific in SON and DJF
250 (Fig. 2c). The “ Q_H Decay” sector reflects the positive covariance between anomalies of SST and
251 MLD. A positive covariance is associated with upwelling processes. When upwelling is
252 enhanced, SST decreases due to more intrusion of cold water from deeper levels. At the same
253 time, temperature around the bottom of the mixed layer decreases more than at the surface. Thus,
254 MLD shoals due to the enhanced stratification induced by anomalous upwelling. Analogous,
255 when upwelling is suppressed, SST increases due to less intrusion of cold water from deeper
256 levels. At the same time, temperature around the bottom of the mixed layer increases more than
257 at the surface. Thus, MLD becomes thicker due to less stratification induced by suppressed
258 upwelling.

259 Horizontal maps of the “ Q_H Decay” occurrence frequency (Fig. 3b,f,j,n) show that this
260 process is dominant in the eastern tropical Pacific. As explained in the previous paragraph, it is
261 consistent with the unique regionality of positive covariance between anomalies of SST and
262 MLD due to the oceanic upwelling zone (Carton et al., 2008; Cronin & Kessler, 2002; Huang et
263 al., 2012; Wang & McPhaden, 2000), resulting in negative anomalies of equivalent heat flux
264 with deeper MLD under climatological heating in the tropics that act to dampen SST anomalies.



265
 266 **Figure 2: Normalized histograms of FDA in 8 selected regions (a. NH Pacific [120°E-100°W, 10°N-60°N], b.**
 267 **NH Atlantic [160°W-0°E, 10°N-60°N], c. EQ Pacific [120°E-70°W, 10°S-10°N], d. EQ Atlantic [70°W-20°E,**
 268 **10°S-10°N], e. EQ Indian Ocean [30°E-120°E, 10°S-25°N], f. SH Pacific [130°E-70°W, 60°S-10°S], g. SH**
 269 **Atlantic [70°W-20°E, 10°S-10°N], and h. SH Indian Ocean [20°E-130°E, 60°S-10°S]). Each color and line width**
 270 **indicates the results for each season separately (DJF [thick, blue], MAM [thin, orange], JJA [thick orange],**
 271 **SON [thin blue], All season [black filled]). Bin size of the histograms is 5°. Vertical lines in each panel**
 272 **indicates the boundary between each sector. The map in upper right corner indicates the area of each selected**
 273 **region.**

274



275

276 **Figure 3: Horizontal maps of occurrence frequencies (Unit: %) in the four sectors for each season. From left**
 277 **to right, the “Q_O Decay”, “Q_H Decay”, “Q_O Growth”, and “Q_H Growth” sectors are displayed, respectively.**
 278 **Each row shows the results in DJF (1st row), MAM (2nd row), JJA (3rd row), and SON (4th row).**

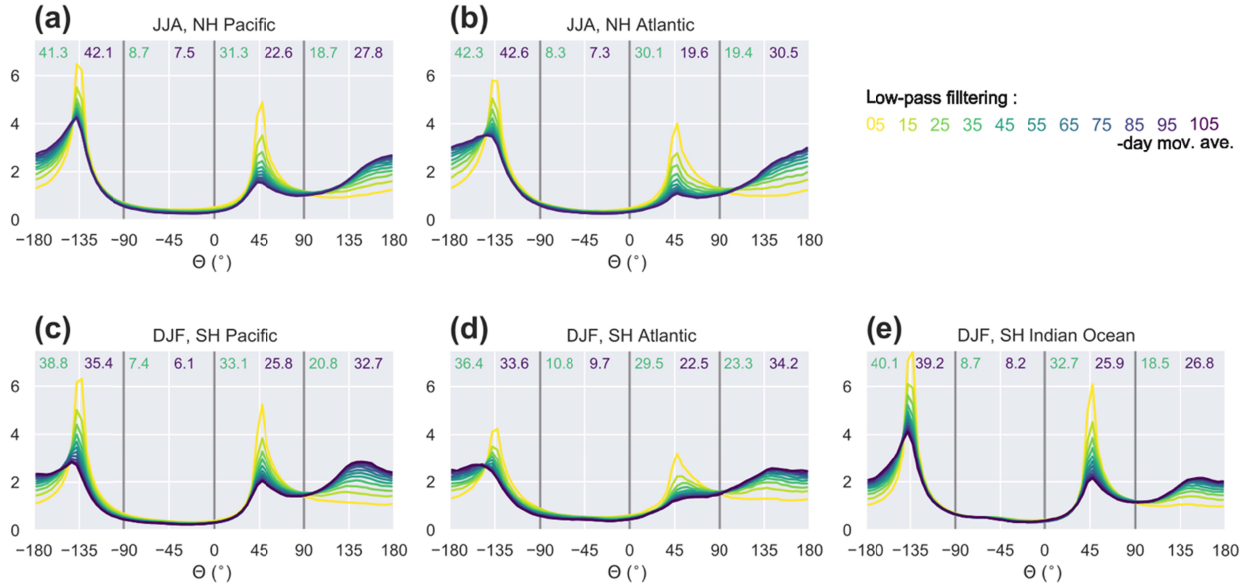
279

280 3.3 Timescale dependence of the FDA histograms

281 Finally, we examine the timescale dependence of the relative contributions of SHF and
 282 MLD anomalies using 5-day mean variables from the SODA 3.4.2 dataset. Focusing on the
 283 summertime extra-tropics, when and where MLD anomalies largely contribute to the growth of
 284 the SST anomaly (Figs. 2 and 3), we compute the FDA histograms using low-pass filtered
 285 variables with different moving window sizes ranging from 15-days to 95-days (Fig. 4). The
 286 results show a clear timescale dependence of the dominant sectors, particularly for “Q_H Growth”
 287 (i.e., $90^\circ < \theta < 180^\circ$). The contribution of the MLD anomaly is very small when no low-pass
 288 filtering is used (i.e., 5-day mean variable). However, the occurrence frequency of “Q_H Growth”
 289 becomes large when the window size is 25-days or 35-days in all selected regions and seasons.
 290 For example, in the summertime North Pacific (Fig. 4a), the occurrence frequency of “Q_H
 291 Growth” increases from 18.7 % to 27.8% and the occurrence frequency of “Q_O Growth”
 292 decreases from 31.3 % to 22.6 % when we change the window size from 5-days to 35-days.

293

294 This suggests that contribution of MLD anomalies is more pronounced on seasonal
 295 timescales than on sub-monthly timescales. This could be explained by the difference in
 296 dominant frequencies between MLD and SHF variability. Specifically, the spectra of SHF and
 297 MLD anomalies correspond to “white noise” and “red noise”, respectively (Fig. S5). Therefore,
 298 the contribution of MLD anomalies is more pronounced on longer timescales. Compared to the
 299 extra-tropics in the summer hemisphere, there is no clear timescale dependence of the
 300 contribution of MLD anomalies in the tropics (Fig. S6).



301

302 **Figure 4: Timescale dependence of the FDA histograms in the extra-tropics in the summer hemisphere (JJA**
 303 **in NH and DJF in SH) using 5-day mean variables from SODA3.4.2. Colored lines show the histogram using**
 304 **different moving averaged variables in the time dimension (legend in the upper right corner of the panel).**
 305 **Colored text (light green and dark purple) at the top of each panel shows the relative frequencies in the four**
 306 **sectors using 5-day and 35-day mean variables, respectively (Unit: %).**

307

308 4 Summary and Discussion

309 To reveal the seasonal and regional characteristics of the role of MLD anomalies in
 310 modulating SST variability, we propose a metric called Flux Divergence Angle (FDA) that
 311 quantifies the relative contributions of anomalies of SHF and MLD anomalies to the month-to-
 312 month variations of SST anomalies. The FDA is based on a metric proposed by Tozuka et al.
 313 (2018). Using the FDA, we investigate the seasonal and regional characteristics of their relative
 314 contributions. The contribution of MLD anomalies has two distinct features. First, MLD
 315 anomalies amplify local SST anomalies particular in the extra-tropics during spring and summer,
 316 relative to the contribution of SHF anomalies. Second, MLD anomalies suppress SST anomalies
 317 particularly in the eastern part of the tropical Pacific during DJF. As discussed in section 3, we
 318 speculate that the opposite role of MLD anomalies is associated with opposite signed
 319 covariances between SST and MLD anomalies due to different formation mechanisms of MLD
 320 (i.e., shoaling MLD by enhanced surface heating in the summertime extra-tropics vs. deepening
 321 MLD by enhanced upwelling in the eastern tropical Pacific). A timescale dependence of
 322 contributions of MLD anomalies in the extra-tropics during summer is also examined, indicating
 323 an enhanced contribution of MLD anomalies on seasonal timescales compared to sub-monthly
 324 timescales due to a large variance of MLD anomalies on longer timescales (red spectrum).

325 Our results show that the spatial pattern with pronounced contributions of MLD
 326 anomalies in the North Pacific during summer is horseshoe-like (Fig. 3). This implies that MLD
 327 anomalies might play a critical role in driving major climate modes in the North Pacific, such as
 328 the Pacific Decadal Oscillation (PDO). Recent papers pointed out the importance of MLD

329 anomalies in modulating major modes of climate variability such as the PDO (Dawe &
330 Thompson, 2007), Atlantic Meridional Mode (Kataoka et al., 2019), and the Atlantic
331 Multidecadal Oscillation (Yamamoto et al., 2020). Kataoka et al. (2019) also revealed that
332 variations in MLD have the potential to more than double the wind-evaporation-SST feedback
333 rate. Thus, the role of MLD anomalies in climate variability should be paid more attention to and
334 its further investigation is needed. In addition, large uncertainties associated with summertime
335 MLD in ocean and coupled general circulation models have been found (Ezer, 2000; Huang et al.,
336 2014) which is a potential source of SST biases (Zhu et al., 2020). Thus, improved understanding
337 of different formation mechanisms of MLD anomalies is required, especially for physical
338 processes associated with the atmospheric-forced MLD variability (Lee et al., 2015; Pookkandy
339 et al., 2016; Ushijima & Yoshikawa, 2019; Yoshikawa, 2015). Finally, we note that our simple
340 metric based on only three variables appears to be a useful diagnostic of the upper ocean
341 representation in climate models.

342

343 **Data Availability Statement**

344 Most of the datasets used in this study can be downloaded from Asia-Pacific Data Research
345 Center; <http://apdrc.soest.hawaii.edu/data/data.php>, which is a part of the International Pacific
346 Research Center at the University of Hawai'i at Mānoa, funded in part by the National Oceanic
347 and Atmospheric Administration (NOAA). Original data sources are listed below; OISSTv2 is
348 from <https://www.ncei.noaa.gov/products/optimum-interpolation-sst>, SODA3.4.2 dataset is from
349 https://www2.atmos.umd.edu/~ocean/index_files/soda3.4.2_mn_download_b.htm. CERES data
350 were obtained from the NASA Langley Research Center CERES ordering tool at
351 https://asdc.larc.nasa.gov/project/CERES/CERES_EBAF_Edition4.1. The global ocean heat flux
352 and evaporation data provided by the Woods Hole Oceanographic Institution OAF flux project
353 (<https://oafux.whoi.edu/data-access/>) were funded by the NOAA Climate Observations and
354 Monitoring (COM) program.

355 **Acknowledgments**

356 This study was supported by the collaborative JICore project between JAMSTEC and IPRC.
357 MFS was supported by NSF grant AGS-2141728 and NOAA's Climate Program Office's
358 Modeling, Analysis, Predictions, and Projections (MAPP) program grant NA20OAR4310445.
359 HA acknowledges the partial support from NOAA/MAPP program grants NA18OAR4310279
360 and NA21OAR4310348. This is IPRC publication X and SOEST contribution Y.

361

362 **References**

363 Alexander, M. A., & Penland, C. (1996). Variability in a Mixed Layer Ocean Model Driven by
364 Stochastic Atmospheric Forcing. *Journal of Climate*, 9(10), 2424–2442.
365 [https://doi.org/10.1175/1520-0442\(1996\)009<2424:VIAMLO>2.0.CO;2](https://doi.org/10.1175/1520-0442(1996)009<2424:VIAMLO>2.0.CO;2)

- 366 Alexander, M. A., Scott, J. D., & Deser, C. (2000). Processes that influence sea surface
367 temperature and ocean mixed layer depth variability in a coupled model. *Journal of*
368 *Geophysical Research: Oceans*, *105*(C7), 16823–16842.
369 <https://doi.org/10.1029/2000jc900074>
- 370 Amaya, D. J., Alexander, M. A., Capotondi, A., Deser, C., Karnauskas, K. B., Miller, A. J., &
371 Mantua, N. J. (2021). Are Long-Term Changes in Mixed Layer Depth Influencing North
372 Pacific Marine Heatwaves? *Bulletin of the American Meteorological Society*, *102*(1), S59–
373 S66. <https://doi.org/10.1175/BAMS-D-20-0144.1>
- 374 Boucharel, J., Timmermann, A., Santoso, A., England, M. H., Jin, F., & Balmaseda, M. A.
375 (2015). A surface layer variance heat budget for ENSO. *Geophysical Research Letters*,
376 *42*(9), 3529–3537. <https://doi.org/10.1002/2015GL063843>
- 377 de Boyer Montégut, C. (2004). Mixed layer depth over the global ocean: An examination of
378 profile data and a profile-based climatology. *Journal of Geophysical Research*, *109*(C12),
379 C12003. <https://doi.org/10.1029/2004JC002378>
- 380 Carton, J. A., Grodsky, S. A., & Liu, H. (2008). Variability of the oceanic mixed layer, 1960-
381 2004. *Journal of Climate*, *21*(5), 1029–1047. <https://doi.org/10.1175/2007JCLI1798.1>
- 382 Carton, J. A., Chepurin, G. A., & Chen, L. (2018). SODA3: A New Ocean Climate Reanalysis.
383 *Journal of Climate*, *31*(17), 6967–6983. <https://doi.org/10.1175/JCLI-D-18-0149.1>
- 384 Cronin, M. F., & Kessler, W. S. (2002). Seasonal and interannual modulation of mixed layer
385 variability at 0°, 110°W. *Deep Sea Research Part I: Oceanographic Research Papers*, *49*(1),
386 1–17. [https://doi.org/10.1016/S0967-0637\(01\)00043-7](https://doi.org/10.1016/S0967-0637(01)00043-7)
- 387 Cronin, M. F., Bond, N. A., Thomas Farrar, J., Ichikawa, H., Jayne, S. R., Kawai, Y., et al.
388 (2013). Formation and erosion of the seasonal thermocline in the Kuroshio Extension

- 389 Recirculation Gyre. *Deep Sea Research Part II: Topical Studies in Oceanography*, 85, 62–
390 74. <https://doi.org/10.1016/j.dsr2.2012.07.018>
- 391 Dawe, J. T., & Thompson, L. A. (2007). PDO-Related Heat and Temperature Budget Changes in
392 a Model of the North Pacific. *Journal of Climate*, 20(10), 2092–2108.
393 <https://doi.org/10.1175/JCLI4229.1>
- 394 Dee, D. P., Uppala, S. M., Simmons, A. J., Berrisford, P., Poli, P., Kobayashi, S., et al. (2011).
395 The ERA-Interim reanalysis: configuration and performance of the data assimilation system.
396 *Quarterly Journal of the Royal Meteorological Society*, 137(656), 553–597.
397 <https://doi.org/10.1002/qj.828>
- 398 Elsberry, R. L., & Garwood, R. W. (1978). Sea-Surface Temperature Anomaly Generation in
399 Relation to Atmospheric Storms. *Bulletin of the American Meteorological Society*, 59(7),
400 786–789. [https://doi.org/10.1175/1520-0477\(1978\)059<0786:SSTAGI>2.0.CO;2](https://doi.org/10.1175/1520-0477(1978)059<0786:SSTAGI>2.0.CO;2)
- 401 Ezer, T. (2000). On the seasonal mixed layer simulated by a basin-scale ocean model and the
402 Mellor-Yamada turbulence scheme. *Journal of Geophysical Research: Oceans*, 105(C7),
403 16843–16855. <https://doi.org/10.1029/2000JC900088>
- 404 Frankignoul, C., & K. Hasselmann. (1977). Stochastic Climate Models, Part II Application to
405 Sea-Surface Temperature Anomalies and Thermocline Variability. *Tell'Us*, 29 (4), 289–305.
- 406 Guan, C., McPhaden, M. J., Wang, F., & Hu, S. (2019). Quantifying the Role of Oceanic
407 Feedbacks on ENSO Asymmetry. *Geophysical Research Letters*, 46(4), 2140–2148.
408 <https://doi.org/10.1029/2018GL081332>
- 409 Hasselmann, K. (1976). Stochastic Climate Models Part I. Theory. *Tell'Us*, 28 (6), 473–85.
- 410 Huang, B., Xue, Y., Wang, H., Wang, W., & Kumar, A. (2012). Mixed layer heat budget of the
411 El Niño in NCEP climate forecast system. *Climate Dynamics*, 39(1–2), 365–381.

- 412 <https://doi.org/10.1007/s00382-011-1111-4>
- 413 Huang, C. J., Qiao, F., & Dai, D. (2014). Evaluating CMIP5 simulations of mixed layer depth
414 during summer. *Journal of Geophysical Research: Oceans*, *119*(4), 2568–2582.
415 <https://doi.org/10.1002/2013JC009535>
- 416 Kataoka, T., Kimoto, M., Watanabe, M., & Tatebe, H. (2019). Wind–Mixed Layer–SST
417 Feedbacks in a Tropical Air–Sea Coupled System: Application to the Atlantic. *Journal of*
418 *Climate*, *32*(13), 3865–3881. <https://doi.org/10.1175/JCLI-D-18-0728.1>
- 419 Lanzante, J. R., & Harnack, R. P. (1983). An investigation of summer sea surface temperature
420 anomalies in the eastern North Pacific Ocean. *Tellus A: Dynamic Meteorology and*
421 *Oceanography*, *35*(4), 256–268. <https://doi.org/10.3402/tellusa.v35i4.11438>
- 422 Lee, E., Noh, Y., Qiu, B., & Yeh, S.-W. (2015). Seasonal variation of the upper ocean
423 responding to surface heating in the North Pacific. *Journal of Geophysical Research:*
424 *Oceans*, *120*(8), 5631–5647. <https://doi.org/10.1002/2015JC010800>
- 425 Loeb, N. G., Doelling, D. R., Wang, H., Su, W., Nguyen, C., Corbett, J. G., et al. (2018). Clouds
426 and the Earth’s Radiant Energy System (CERES) Energy Balanced and Filled (EBAF) Top-
427 of-Atmosphere (TOA) Edition-4.0 Data Product. *Journal of Climate*, *31*(2), 895–918.
428 <https://doi.org/10.1175/JCLI-D-17-0208.1>
- 429 Morioka, Y., Tozuka, T., & Yamagata, T. (2010). Climate variability in the southern Indian
430 Ocean as revealed by self-organizing maps. *Climate Dynamics*, *35*(6), 1059–1072.
431 <https://doi.org/10.1007/s00382-010-0843-x>
- 432 Morioka, Y., Tozuka, T., & Yamagata, T. (2011). On the Growth and Decay of the Subtropical
433 Dipole Mode in the South Atlantic. *Journal of Climate*, *24*(21), 5538–5554.
434 <https://doi.org/10.1175/2011JCLI4010.1>

- 435 Paulson, C. A., & Simpson, J. J. (1977). Irradiance Measurements in the Upper Ocean. *Journal*
436 *of Physical Oceanography*, 7(6), 952–956. [https://doi.org/10.1175/1520-](https://doi.org/10.1175/1520-0485(1977)007<0952:IMITUO>2.0.CO;2)
437 0485(1977)007<0952:IMITUO>2.0.CO;2
- 438 Pookkandy, B., Dommenget, D., Klingaman, N., Wales, S., Chung, C., Frauen, C., & Wolff, H.
439 (2016). The role of local atmospheric forcing on the modulation of the ocean mixed layer
440 depth in reanalyses and a coupled single column ocean model. *Climate Dynamics*, 47(9–10),
441 2991–3010. <https://doi.org/10.1007/s00382-016-3009-7>
- 442 Qiu, B., & Kelly, K. A. (1993). Upper-Ocean Heat Balance in the Kuroshio Extension Region.
443 *Journal of Physical Oceanography*, 23(9), 2027–2041. [https://doi.org/10.1175/1520-](https://doi.org/10.1175/1520-0485(1993)023<2027:UOHBIT>2.0.CO;2)
444 0485(1993)023<2027:UOHBIT>2.0.CO;2
- 445 Reynolds, R. W., Rayner, N. A., Smith, T. M., Stokes, D. C., & Wang, W. (2002). An Improved
446 In Situ and Satellite SST Analysis for Climate. *Journal of Climate*, 15(13), 1609–1625.
447 [https://doi.org/10.1175/1520-0442\(2002\)015<1609:AIISAS>2.0.CO;2](https://doi.org/10.1175/1520-0442(2002)015<1609:AIISAS>2.0.CO;2)
- 448 Ruddick, B. (1983). A practical indicator of the stability of the water column to double-diffusive
449 activity. *Deep Sea Research Part A. Oceanographic Research Papers*, 30(10), 1105–1107.
450 [https://doi.org/10.1016/0198-0149\(83\)90063-8](https://doi.org/10.1016/0198-0149(83)90063-8)
- 451 Santoso, A., Sen Gupta, A., & England, M. H. (2010). Genesis of Indian Ocean Mixed Layer
452 Temperature Anomalies: A Heat Budget Analysis. *Journal of Climate*, 23(20), 5375–5403.
453 <https://doi.org/10.1175/2010JCLI3072.1>
- 454 Sugimoto, S., & Kako, S. (2016). Decadal Variation in Winter Mixed Layer Depth South of the
455 Kuroshio Extension and Its Influence on Winter Mixed Layer Temperature. *Journal of*
456 *Climate*, 29(3), 1237–1252. <https://doi.org/10.1175/JCLI-D-15-0206.1>
- 457 Takahashi, N., Richards, K. J., Schneider, N., Annamalai, H., Hsu, W., & Nonaka, M. (2021).

- 458 Formation Mechanism of Warm SST Anomalies in 2010s Around Hawaii. *Journal of*
459 *Geophysical Research: Oceans*, 126(11), 1–14. <https://doi.org/10.1029/2021JC017763>
- 460 Tozuka, T., S. Ohishi, and M. F. Cronin. (2018). A Metric for Surface Heat Flux Effect on
461 Horizontal Sea Surface Temperature Gradients., *Climate Dynamics*, 51 (1–2), 547–61
- 462 Ushijima, Y., & Yoshikawa, Y. (2019). Mixed Layer Depth and Sea Surface Warming under
463 Diurnally Cycling Surface Heat Flux in the Heating Season. *Journal of Physical*
464 *Oceanography*, 49(7), 1769–1787. <https://doi.org/10.1175/JPO-D-18-0230.1>
- 465 Wang, W., & McPhaden, M. J. (2000). The surface-layer heat balance in the Equatorial Pacific
466 Ocean Part II: Interannual variability. *Journal of Physical Oceanography*, 30(11), 2989–
467 3008. [https://doi.org/10.1175/1520-0485\(2001\)031<2989:TSLHBI>2.0.CO;2](https://doi.org/10.1175/1520-0485(2001)031<2989:TSLHBI>2.0.CO;2)
- 468 Yamaguchi, R., & Suga, T. (2019). Trend and Variability in Global Upper-Ocean Stratification
469 Since the 1960s. *Journal of Geophysical Research: Oceans*, 124(12), 8933–8948.
470 <https://doi.org/10.1029/2019JC015439>
- 471 Yamamoto, A., Tatebe, H., & Nonaka, M. (2020). On the Emergence of the Atlantic
472 Multidecadal SST Signal: A Key Role of the Mixed Layer Depth Variability Driven by
473 North Atlantic Oscillation. *Journal of Climate*, 33(9), 3511–3531.
474 <https://doi.org/10.1175/JCLI-D-19-0283.1>
- 475 Yokoi, T., Tozuka, T., & Yamagata, T. (2012). Seasonal and Interannual Variations of the SST
476 above the Seychelles Dome. *Journal of Climate*, 25(2), 800–814.
477 <https://doi.org/10.1175/JCLI-D-10-05001.1>
- 478 Yoshikawa, Y. (2015). Scaling surface mixing/mixed layer depth under stabilizing buoyancy
479 flux. *Journal of Physical Oceanography*, 45(1), 247–258. [https://doi.org/10.1175/JPO-D-](https://doi.org/10.1175/JPO-D-13-0190.1)
480 13-0190.1

- 481 You, Y. (2002). A global ocean climatological atlas of the Turner angle: implications for double-
482 diffusion and water-mass structure. *Deep Sea Research Part I: Oceanographic Research*
483 *Papers*, 49(11), 2075–2093. [https://doi.org/10.1016/S0967-0637\(02\)00099-7](https://doi.org/10.1016/S0967-0637(02)00099-7)
- 484 Yu, L., Jin, X., & Robert, A. W. (2008). *Multidecade Global Flux Datasets from the Objectively*
485 *Analyzed Air-sea Fluxes (OAFlux) Project: Latent and Sensible Heat Fluxes, Ocean*
486 *Evaporation, and Related Surface Meteorological Variables*. Woods Hole Oceanographic
487 *Institution OAFlux Project Technical Report (OA-2008-01)*. [https://doi.org/10.1007/s00382-](https://doi.org/10.1007/s00382-011-1115-0)
488 [011-1115-0](https://doi.org/10.1007/s00382-011-1115-0)
- 489 Zhu, Y., & Zhang, R.-H. (2018). Scaling wind stirring effects in an oceanic bulk mixed layer
490 model with application to an OGCM of the tropical Pacific. *Climate Dynamics*, 51(5–6),
491 1927–1946. <https://doi.org/10.1007/s00382-017-3990-5>
- 492 Zhu, Y., Zhang, R.-H., & Sun, J. (2020). North Pacific Upper-Ocean Cold Temperature Biases in
493 CMIP6 Simulations and the Role of Regional Vertical Mixing. *Journal of Climate*, 33(17),
494 7523–7538. <https://doi.org/10.1175/JCLI-D-19-0654.1>
- 495

